THE ASTROPHYSICAL JOURNAL, Vol. 160, May 1970


# OH RADIO EMISSION ASSOCIATED WITH INFRARED STARS

W. J. WILSON AND A. H. BARRETT
Research Laboratory of Electronics,* Massachusetts Institute of Technology

AND

J. M. MORAN
Massachusetts Institute of Technology, Lincoln Laboratory†
*Received 1969 October 1; revised 1969 November 14*

## ABSTRACT

A search of sixty infrared stars for OH emission at 1612 MHz has been made. OH emission was detected from seven of these objects, and their spectra and polarization properties have been measured. These OH sources are the first to be identified with stellar objects. Also, seven T Tauri and eight known red-giant stars were observed, with negative results. The OH source in NML Cygnus was studied with a very-long-baseline interferometer and found to be coincident in position with the infrared star within 5″ and to have individual spectral features within 2″ of one another with characteristic sizes of 0″.08. The characteristics of the OH emission are best explained by a partially saturated maser pumped by near-infrared radiation. A model of an evolved, very luminous red-giant star with an expanding atmosphere is proposed to explain the observed properties.

## I. INTRODUCTION

Following the discovery of OH emission from infrared (IR) stars in 1968 July (Wilson and Barrett 1968), a joint program was undertaken with the infrared astronomy group at the California Institute of Technology (CIT) to study the OH and IR properties of these sources. The purpose of this paper is to present the results of the initial phase of the OH observations and to present a possible model to explain the OH emission from these sources. The IR stars observed in this program were discovered during the 2-$\mu$ sky survey of the California Institute of Technology (Neugebauer and Leighton 1969), and the IR properties of these stars are the subject of another paper by Hyland, Becklin, Frogel, and Neugebauer (1970).

Sixty IR stars have been surveyed for OH emission at 1612 MHz. Twenty-four of these stars have been observed at all four OH frequencies. OH emission has been positively detected from seven of the IR stars. Seven T Tauri and eight well-known red-giant stars were also surveyed for OH, with negative results. The OH emission associated with these IR stars has six distinguishing properties:

1. The OH emission is strongest at the 1612-MHz satellite-line frequency.
2. The 1612-MHz emission occurs in two main ranges of velocity.
3. The 1612-MHz emission is very weakly polarized, if at all.
4. Main-line emission is most likely to occur at 1667 MHz.
5. There is no OH emission at 1720 MHz, the other satellite-line frequency.
6. There is no detectable continuum radio source at the location of the OH/IR source.

In addition to the single-antenna observations reported, measurements were made with a very-long-baseline interferometer (VLBI) on the strong OH source associated with the IR source NML Cygnus. The spatial structure of the OH emission was found to be very complex. This source has many features with sizes of ~0″.1 located within 2″ of one another.

* This work was supported in part by the National Aeronautics and Space Administration (grant NGL 22-009-016) and the National Science Foundation (grant GP-13056).

† This work was sponsored by the Department of the Air Force.

In § II, the equipment and the observational procedures are described. In § III, details of the sources detected and a summary of the negative observations are presented. In § IV the theory of IR pumping of the OH maser is applied to explain the observed OH emission, and possible geometrical models are discussed. Based on the observed properties, a model of an evolved, very luminous, red-giant star with an expanding atmosphere is proposed to explain the OH emission.

## II. EQUIPMENT AND OBSERVING PROCEDURE

### *a) Single-Antenna Observations*

The single-antenna observations reported here were made with the 140-foot (43-m) radio telescope of the National Radio Astronomy Observatory (NRAO), located in Green Bank, West Virginia, during 1968 June/July, October, and December. In June/July and December, the antenna was illuminated with a feed horn with two orthogonal linearly polarized probes. It was possible to rotate this feed to measure the different angles of linear polarization. Circular polarization was achieved by appropriately combining the two orthogonal linearly polarized signals. The measured isolation between right- and left-circular polarization was greater than 17 db. In October, the antenna was illuminated with a vertically polarized feed horn. The intrinsic polarization of the system was measured by using the unpolarized continuum source 3C 274, and the differences in system gain at each polarization were less than 5 percent. The first stage of the receiver was an uncooled parametric amplifier, giving a total system-noise temperature of 250° K in June/July and December and 350° K in October. Spectral-line processing was performed by using the NRAO 400-channel autocorrelator.

The observational procedure during the search for new OH sources was to switch frequencies between two adjacent frequency bands. The advantage of this method over normal frequency switching is that it is possible to cover twice the velocity range with the same frequency resolution during one scan. For measurement of the properties of the detected sources, a frequency-switching technique with the reference band below and above the signal band was used.

To complete the data coverage, observations at 1665 and 1667 MHz on the source IRC−20197 were made in 1969 April with the Harvard College Observatory's 84-foot (26-m) Agassiz radio telescope. Data were taken with both right- and left-circularly polarized feeds.

Flux calibration was made by using the source 3C 274. The unpolarized flux $S_0$ of 3C 274 was taken to be 266 flux units (f.u.) at 1000 MHz with a spectral index of −0.81 (Kellermann and Pauliny-Toth 1969). The ratio of the flux-to-antenna temperature for an unpolarized source varied between 3.3 and 4.0 f.u. $^\circ$ K$^{-1}$ for the different observing periods and frequencies. Measurements of polarization were made by measuring spectra in either linear or circular polarization and then combining the results to obtain the Stokes parameters (Ball and Meeks 1968). Right-circular polarization is defined as the rotation of the electric vector in a clockwise manner when viewed along the direction of propagation. Other parameters, such as the degree of polarization and the polarization angle, were derived directly from the Stokes parameters.

### *b) VLBI Observations*

Simultaneous observations of NML Cyg were made in 1968 October and 1969 January with the 140-foot antenna at NRAO and the 120-foot antenna of the Haystack research facility of Lincoln Laboratory, MIT. This interferometric technique has been previously used to probe the structure of other OH sources (Moran *et al.* 1968). To implement the interferometer, the 30-MHz signals from the OH receivers on each telescope were processed through video converters, clipped, sampled, and recorded digitally. The recording terminals were built jointly by the National Radio Astronomy Observatory and the

Arecibo Ionospheric Observatory (Bare *et al.* 1967). All of the local oscillators were phase-locked to hydrogen-maser frequency standards to avoid introducing phase noise into the signals.

The feeds on both antennas were linear in the vertical sense for compatibility with another experiment so that the polarizations achieved were not collinear, especially for sources near the zenith at either site. By avoiding the 3-hour period near transit, however, the feed polarizations were aligned within 15°. With the use of vertical polarization, the position angle of the polarization vector on the sky changes with local hour angle. NML Cygnus appears to be almost unpolarized at 1612 MHz, so this effect may be of no consequence. If the source is made up of polarized features that overlap in velocity but are spatially separated, then the interference spectra observed will be affected by the polarization of the antennas. This possibility has not been checked.

The data on the two tapes recorded simultaneously were cross-correlated over time intervals of 0$^s$.02 on a general-purpose computer. They were then synchronously demodulated at the expected fringe rate and at ten other frequencies slightly offset from the expected fringe rate. The resulting correlation functions were transformed to yield the interference spectra as a function of frequency and fringe rate. The complex fringe visibilities were obtained by dividing the interference spectra by the geometric mean of the individual power spectra. This normalization procedure does not require knowledge of specific system parameters, e.g., system temperature or antenna efficiency.

## III. OBSERVATIONS

The search for OH emission from IR sources was begun for two main reasons: (1) the discovery by Raimond and Eliasson (1967) that the OH emission source in the Orion Nebula was at the same position as the IR point source of Becklin and Neugebauer (1967), and (2) the theory that the OH molecule could be excited for masering by IR radiation, as originally proposed by Shklovskii (1967) and later developed by Litvak (1969*a*). Our initial observations were made at all four of the OH frequencies, but after the characteristics of the emission became apparent, the search observations were made only at 1612 MHz.

The IR stars observed in this work were discovered during the CIT infrared survey (Neugebauer, Martz, and Leighton 1965; Neugebauer and Leighton 1969). The stars were selected for observation on the basis of redness. Almost all sources on the CIT list with $I-K$ greater than 6.5 mag were observed. These cool sources were selected because they would provide a large flux near 2.8 $\mu$ for the infrared excitation of the OH maser and the conditions near the source might be suitable for the OH masering cloud. There are two OH/IR sources, VY CMa (Eliasson and Bartlett 1969) and IR+10406 (R Aql), which have $I-K$ magnitudes of 5.6 and 5.0, respectively, making them the "hottest" OH/IR sources yet found. It should be noted that these are the only two OH/IR sources from which microwave $H_2O$ emission has been detected at the present time (Turner *et al.* 1970). Failure to detect OH emission from seven T Tauri and eight red-giant stars, as mentioned, provides some information about the range of conditions under which OH emission can be expected. The typical $I-K$ magnitude of these T Tauri and red-giant stars is 2.0 (Mendoza V. 1968; Johnson *et al.* 1966). Future observations will include samples of the sources with $I-K$ between 2.0 and 5.0.

Table 1 gives a list of all known OH sources associated with IR sources. Included for the sake of completeness are three sources discovered by other observers: Orion A, VY CMa, and ON-4 (Ellder, Ronnang, and Winnberg 1969). Although no IR star has been detected at the position of ON-4, it was included because it has the six characteristics of OH/IR emission. Orion A does not have all six of the characteristics; however, it is coincident with the Orion IR point source (Raimond and Eliasson 1967). The names of the IR stars are from the CIT infrared catalog (Neugebauer and Leighton 1969). The

results of the observations of the sources with OH emission reported here are summarized in Table 2.

All of the OH/IR stars except Orion A, VY CMa, ON-4, and NML Cyg have been identified as Mira-type variables (Hyland, Becklin, Frogel, and Neugebauer 1970). VY CMa is an irregular variable. It is interesting that the average galactic latitude of these OH/IR sources and that of all Mira variables is approximately 20° (Allen 1963). None of the observed sources has a discrete continuum radio source at the observed position with an 18-cm flux greater than 10 f.u. A brief discussion of the details of the observations for each source will be presented in the following paragraphs.

### *a) NML Cygnus*

Neugebauer *et al.* (1965) discovered the source NML Cyg during the CIT infrared survey. It is one of the brightest IR stars at 10 $\mu$ and also one of the reddest stars with an $I-K$ magnitude of 8.2. If its distance is 500 pc, its luminosity would be $5 \times 10^4 L_\odot$ (Stein *et al.* 1969). Johnson (1968) and Hyland, Becklin, Neugebauer, and Wallerstein

TABLE 1

OH/IR SOURCES: POSITIVE RESULTS

| Source | R.A. (1950) | Decl. (1950) | $l^{II}$ | $b^{II}$ | Remarks |
|---|---|---|---|---|---|
| IRC+10011.... | $01^h03^m49^s0$ | +12°18′.7 | 128.64 | −50.11 | CIT-3 |
| NML Tau..... | 03 50 46.0 | +11 15.7 | 177.95 | −31.42 | IRC+10050 |
| IRC+50137.... | 05 07 20.0 | +52 48.8 | 156.44 | + 7.83 | |
| Orion A..... | 05 32 46.8 | −05 24.4 | 208.99 | −19.38 | IR point source |
| VY CMa..... | 07 20 53.0 | −25 40.4 | 239.35 | − 5.07 | IRC−30087 |
| IRC−20197.... | 09 42 56.0 | −21 48.1 | 255.80 | +23.35 | |
| IRC+20281.... | 15 25 32.0 | +19 44.1 | 29.51 | +53.48 | WX Ser, CIT-7 |
| IRC+10406.... | 19 03 58.0 | +08 9.1 | 41.95 | + 0.45 | R Aql |
| ON-4..... | 20 26 54.0 | +38 56.0 | 77.90 | + 0.18 | No IR star detected |
| NML Cyg..... | 20 44 33.9 | +39 55.9 | 80.80 | − 1.92 | IRC+40448 |

(1969) have concluded that NML Cyg is a highly reddened M supergiant. NML Cygnus has not been observed to vary at 2 $\mu$ (Neugebauer 1969); however, Low (1969) reported that the 10-$\mu$ emission has been observed to decrease by 1 mag during the last 5 years. Forbes (1967) has found that the IR radiation is significantly polarized (4 percent) and has concluded that the majority of this polarization was due to the interstellar material in the Cygnus region. Some of the reddening of the spectrum may also be due to this material. From the shape of the IR spectrum, Hyland, Becklin, Neugebauer, and Wallerstein (1969) proposed a model for NML Cyg that comprises a central star at a temperature of 2500° K surrounded by a dense cloud of interstellar particles which converts the stellar radiation to the IR wavelengths. The temperature of the interstellar particles varies from 600° to 250° K progressing outward from the center. As will be seen, the OH observations are consistent with a model for this object in which the central star is obscured by material flowing from the star and the OH emission originates in the outer tenuous atmosphere of the star.

OH emission from NML Cyg is the strongest that has been found. The 1612-, 1665-, and 1667-MHz spectra are shown in Figures 1 and 4. No emission was detected at 1720 MHz to a limit of 1 f.u. The 1612-MHz emission occurs over a range of 46 km sec$^{-1}$ in two distinct widely spaced intervals, −30 to −5 km sec$^{-1}$ and 4 to 25 km sec$^{-1}$. Each velocity range of emission has many separate features, as is clearly seen in the high-resolution spectra in Figures 2 and 3.

TABLE 2

SUMMARY OF POSITIVE RESULTS

| Source | Date (1968) | Frequency (MHz) | Antenna Polarization | Velocity Range (km sec$^{-1}$) | Bandwidth Resolution (kHz) | RMS (f.u.) | Results |
|---|---|---|---|---|---|---|---|
| IRC+10011.. | July | 1612 | $S_0$ | − 95, + 95 | 3.1 | 0.6 | †$S$=21 f.u. at −9.3 and 27 km s$^{-1}$, otherwise $S$<1.5 f.u. |
| | December | 1612 | Linear | −200, +200 | 4.0 | 0.5 | †$S$=9 f.u. at −9.5 and 26 km s$^{-1}$, otherwise $S$<1.5 f.u. |
| | December | 1612 | $S_0$ | − 40, + 60 | 3.1 | 0.2 | †$S$=17.2 f.u. at −9.7 km s$^{-1}$, $S$=16.4 at 26.7 km s$^{-1}$, otherwise $S$<0.6 f.u. |
| | July | 1665 | $S_0$ | − 45, + 45 | 3.1 | 0.4 | $S$<1.1 f.u. |
| | December | 1665 | Linear | −195, +195 | 4.0 | 0.5 | $S$<1.6 f.u. |
| | July | 1667 | $S_0$ | − 45, + 50 | 3.1 | 0.6 | †$S$=1.7 f.u. at −9 km s$^{-1}$, $S$=2.5 f.u. at 26 km s$^{-1}$, otherwise $S$<1.2 f.u. |
| | December | 1667 | Linear | −195, +195 | 6.0 | 0.5 | †$S$=1.3 f.u. at −10 km s$^{-1}$, $S$=1.5 f.u. at 26 km s$^{-1}$, otherwise $S$<1.2 f.u. |
| | July | 1720 | $S_0$ | − 45, + 45 | 3.1 | 0.4 | $S$<1.1 f.u. |
| NML Tau.... | June | 1612 | $S_0$ | − 95, + 95 | 3.1 | 0.5 | †$S$=2 f.u. at 17.4 and 50.4 km s$^{-1}$, otherwise $S$<1.3 f.u. |
| | December | 1612 | Linear | −200, +200 | 3.9 | 0.4 | ?$S$=1.1 f.u. at 50 km s$^{-1}$, otherwise $S$<1 f.u. |
| | June | 1665 | $S_0$ | − 90, + 90 | 3.1 | 0.4 | $S$<1.1 f.u. |
| | December | 1665 | Linear | −195, +195 | 3.9 | 0.4 | $S$<1 1 f.u., ?$S$=1 f.u., at 70 km s$^{-1}$? |
| | July | 1667 | $S_0$ | − 90, + 90 | 3.1 | 0.5 | †$S$=1.8 f.u. at 15 km s$^{-1}$, otherwise $S$<1.1 f.u. |
| | December | 1667 | Linear | −195, +195 | 3.9 | 0.4 | $S$<1.1 f.u. |
| | June | 1720 | $S_0$ | − 90, + 90 | 3.1 | 0.4 | $S$<1.3 f.u. |
| IRC+50137.. | December | 1612 | Linear | −200, +200 | 4.0 | 0.7 | †$S$=2.4 f.u. at −14 km s$^{-1}$, $S$=4 f.u. at 19.5 km s$^{-1}$, otherwise $S$<2 f.u. |
| | December | 1612 | $S_0$ | − 20, + 30 | 1.5 | 0.6 | †$S$=3.6 f.u. at −13.9 km s$^{-1}$, $S$=10 f.u. at 19.8 km s$^{-1}$, otherwise $S$<1.6 f.u. |
| | October | 1665 | Vertical | − 90, + 90 | 3.1 | 0.3 | $S$<0.9 f.u. |
| | December | 1665 | Linear | −195, +195 | 4.0 | 0.6 | $S$<2 f.u. |
| | October | 1667 | Vertical | − 90, + 90 | 3.1 | 0.3 | $S$<0.9 f.u., ?$S$=0.8 f.u. at −6 km s$^{-1}$? |
| | December | 1667 | Linear | −195, +195 | 4.0 | 0.6 | $S$<1.5 f.u., ?$S$=1.2 f.u. at −6 km s$^{-1}$? |
| | December | 1720 | Linear | −190, +190 | 4.0 | 0.5 | $S$<1.4 f.u. |
| IRC−20197.. | December | 1612 | Linear | −200, +200 | 4.0 | 0.6 | †$S$=5 f.u. at 26.5 km s$^{-1}$, $S$=3 f.u. at 51 km s$^{-1}$, otherwise $S$<1.6 f.u. |
| | December | 1612 | $S_0$ | − 10, + 90 | 3.1 | 0.4 | †$S$=7.5 f.u. at 27 km s$^{-1}$, $S$=5.7 f.u. at 51 km s$^{-1}$, otherwise $S$<1.2 f.u. |
| | April | 1665 | $S_0$ | + 18, + 62 | 6.0 | 1.2 | $S$<5 f.u. |
| | April* | 1667 | $S_0$ | + 18, + 62 | 6.0 | 1.2 | $S$<5 f.u. |
| | December | 1720 | Linear | −190, +190 | 4.0 | 0.6 | $S$<2 f.u. |

* 1969.

† Positive detection.

TABLE 2—*Continued*

| Source | Date (1968) | Frequency (MHz) | Antenna Polarization | Velocity Range (km sec$^{-1}$) | Bandwidth Resolution (kHz) | RMS (f.u.) | Results |
|---|---|---|---|---|---|---|---|
| IRC+20281.. | July | 1612 | $S_0$ | − 25, + 25 | 1.5 | 0.5 | †$S$=2.5 f.u. at −1.4 km s$^{-1}$, $S$=1.6 f.u. at 13.4 km s$^{-1}$, otherwise $S$<1.4 f.u. |
| | December | 1612 | Linear | −200, +200 | 4.0 | 0.3 | †$S$=0.8 f.u. at −0.5 km s$^{-1}$, $S$=1 f.u. at 13.2 km s$^{-1}$, otherwise $S$<0.8 f.u. |
| | December | 1665 | Linear | −195, +195 | 4.0 | 0.7 | $S$<2 f.u., ?$S$=2 f.u. at −115, −170 km s$^{-1}$. |
| | December | 1665 | $S_0$ | − 50, + 50 | 3.1 | 0.4 | †$S$=1.2 f.u. at −1 km s$^{-1}$, otherwise $S$<0.8 f.u. |
| | July | 1667 | $S_0$ | − 50, + 50 | 3.1 | 0.5 | †$S$=1.4 f.u. at −0.4 km s$^{-1}$, ?$S$=1 f.u. at −19.4, otherwise $S$< 1 f.u. |
| | December | 1667 | Linear | −195, +195 | 4.0 | 0.6 | ?$S$=1 f.u. at −10, −1, 9, and 53 km s$^{-1}$, otherwise $S$<1 f.u. |
| | July | 1720 | $S_0$ | − 50, + 50 | 3.1 | 0.4 | $S$<1.2 f.u. |
| | December | 1720 | Linear | −190, +190 | 4.0 | 1.0 | $S$<2.8 f.u. |
| IRC+10406.. | December | 1612 | Linear | −200, +200 | 4.0 | 0.7 | †$S$=34 f.u. at 53 km s$^{-1}$, ?$S$=1.6 f.u. at −96, 3, and 177 km s$^{-1}$, otherwise $S$<1.6 f.u. |
| | December | 1612 | $S_0$ | + 25, + 75 | 1.5 | 0.4 | †$S$=4 f.u. at 43.4 km s$^{-1}$, $S$=72 f.u. at 53.8 km s$^{-1}$, otherwise $S$< 1 f.u. |
| | December | 1665 | Linear | −195, +195 | 4.0 | 0.5 | $S$<1.4 f.u. |
| | December | 1667 | Linear | −195, +195 | 4.0 | 0.5 | †$S$=1.9 f.u. at 42.6 km s$^{-1}$, otherwise $S$< 1.4 f.u. |
| | December | 1720 | Linear | −190, +190 | 4.0 | 0.7 | $S$<2.1 f.u. |
| NML Cyg.... | July | 1612 | Linear | −210, +210 | 7.8 | 0.7 | †$S$=217 f.u. at −25 km s$^{-1}$, $S$=81 f.u. at 21 km s$^{-1}$. |
| | July | 1612 | Linear | − 33, + 33 | 0.4 | 1.0 | †$S$=310 f.u. at −23.9 km s$^{-1}$, $S$=91 f.u. at at 21.5 km s$^{-1}$. |
| | December | 1612 | Linear | − 32, + 27 | 0.8 | 0.8 | †$S$=301 f.u. at −23.9 km s$^{-1}$, $S$=97 f.u. at 21.5 km s$^{-1}$. |
| | July | 1665 | $S_0$ | − 30, − 6 | 0.8 | 0.2 | †$S$=2.2 f.u. at −12.7 km s$^{-1}$, $S$=14.4 f.u. at −19.6 km s$^{-1}$, otherwise $S$<0.8 f.u. |
| | December | 1665 | Linear | −195, +195 | 4.0 | 0.7 | †$S$=2 f.u. at −13.4 km s$^{-1}$, $S$=2.7 f.u. at −20.4 km s$^{-1}$, otherwise $S$<1.5 f.u. |
| | December | 1665 | $S_0$ | − 30, + 19 | 1.6 | 0.4 | †$S$=1.9 f.u. at −13 km s$^{-1}$, $S$=11 f.u. at −19.6 km s$^{-1}$, otherwise $S$<1 f.u. |
| | July | 1667 | $S_0$ | − 48, + 48 | 3.0 | 0.2 | †$S$=1.1 f.u. at 10–18 and 25 km s$^{-1}$, otherwise $S$<0.7 f.u. |
| | December | 1667 | Linear | −195, +195 | 4.0 | 0.3 | †$S$=0.9 f.u. at 11–17 and 25 km s$^{-1}$, otherwise $S$<0.8 f.u. |
| | July | 1720 | $S_0$ | − 95, + 95 | 3.1 | 0.2 | $S$<0.7 f.u. |

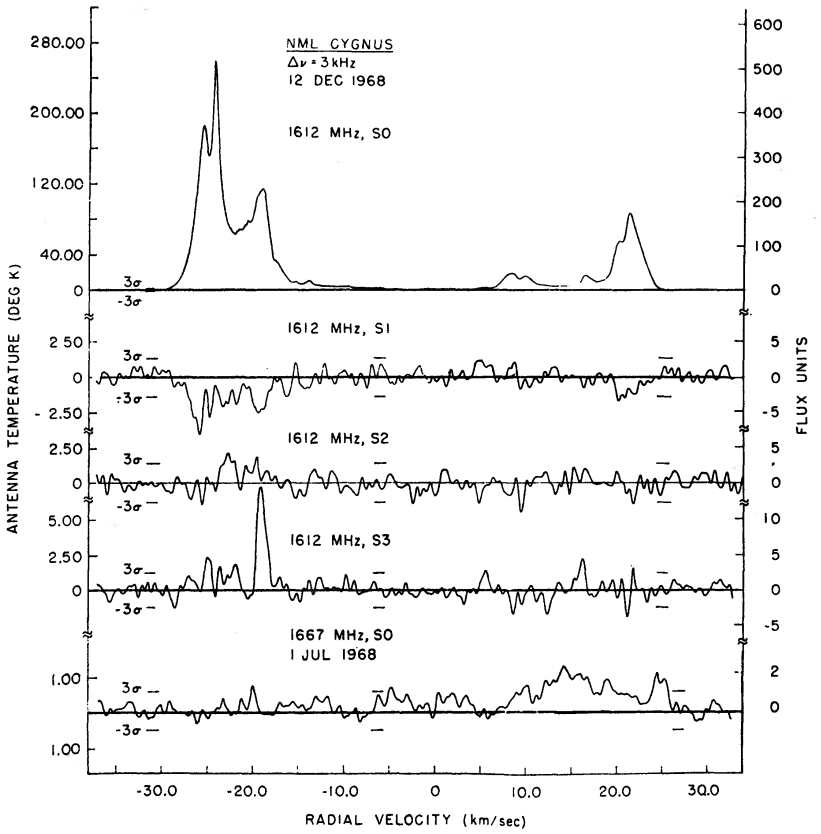


FIG. 1.—The 1612- and 1667-MHz spectra of NML Cyg. $S_0$, $S_1$, $S_2$, and $S_3$ are the Stokes parameters. To convert the given local-standard-of-rest (LSR) velocities to heliocentric velocities, add $-16.5$ km sec$^{-1}$.

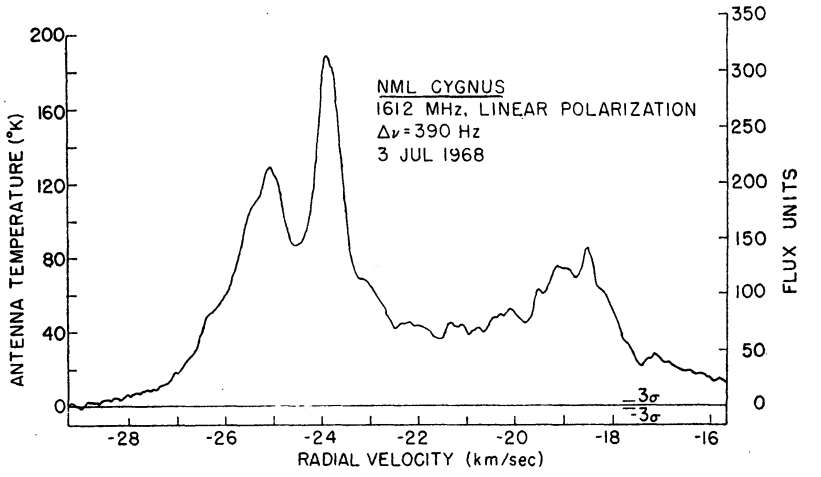


FIG. 2.—High-resolution 1612-MHz spectrum of NML Cyg centered at $-22$ km sec$^{-1}$

The complete set of Stokes parameters was measured for the 1612-MHz emission (Fig. 1), and the circular polarization was measured for the 1665-MHz (Fig. 4) and the 1667-MHz emission. The polarization data for the 1612- and 1665-MHz emission are summarized in Table 3. The 1667-MHz emission had less than 15 percent circular polarization. Three immediate conclusions can be made from these polarization measurements. (1) The 1612- and 1667-MHz emission is mainly unpolarized (less than 10 and 15 percent, respectively), while the 1665-MHz emission is 60 percent left-circularly

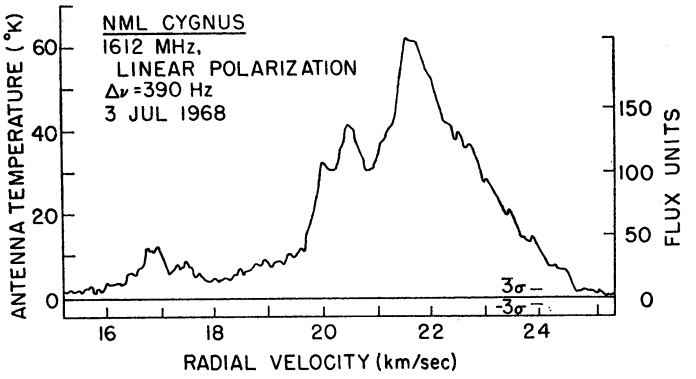


FIG. 3.—High-resolution 1612-MHz spectrum of NML Cyg centered at +20 km sec$^{-1}$

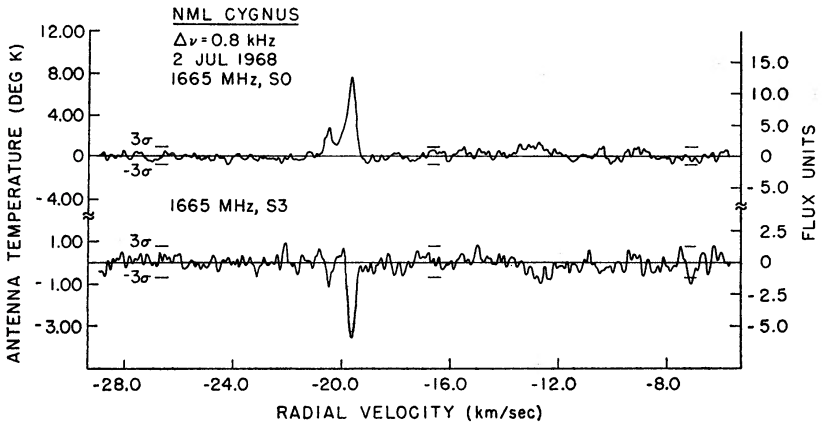


FIG. 4.—The 1665-MHz spectrum of NML Cyg. $S_0$ and $S_3$ are the Stokes parameters.

polarized. (2) At 1612 MHz the −20 km sec$^{-1}$ features have approximately 3 percent linear polarization across the velocity range −25 to −16 km sec$^{-1}$, while the +20 km sec$^{-1}$ features have only 1.5 percent linear polarization across the narrow velocity range 20–22 km sec$^{-1}$. This is strong evidence that the microwave polarization is intrinsic to the source. (3) As seen in Figure 1, the 1612-MHz emission has a small amount of right-circular polarization at the velocity of −19.2 km sec$^{-1}$, which is very close in velocity to the 1665-MHz emission at −19.6 km sec$^{-1}$.[1]

During the period 1968 June 30 to December 12, the OH emission from NML Cyg was constant within 2 percent. Thus NML Cyg does not appear to be a variable in either its 2-$\mu$ IR or its OH emission over this 6-month period.

[1] The rest frequencies used were 1612.231 and 1665.401 MHz.

Figure 5 shows the projected interferometer baselines corresponding to the interference spectra obtained on NML Cyg on 1968 October 11 and 12. The eight spectra are shown in Figure 6. The solid spectrum shown on each plot is the geometric mean spectrum computed from the individual tapes. The dotted curve is the spectrum obtained from cross-correlating the tapes. The fringe rates at which the major features have maximum power are shown. At any velocity the fringe amplitude is the ratio of the two functions. The fringe phase is also shown with a solid line through the portions where there is enough signal to make it significant. There are four points per resolution interval, so the phase appears continuous even where it is only random noise.

TABLE 3

SUMMARY OF POLARIZATION DATA ON NML CYGNUS

| | 1612 MHz | | | | 1665 MHz, |
|---|---|---|---|---|---|
| VELOCITY (km sec$^{-1}$) | Percent Linear | P.A.* | Percent Circular | Total Percent | PERCENT CIRCULAR |
| −25.5 | 2 | 90°±10° | < 0.3 | 2 | ... |
| −25.0 | <3 | ... | 1.5 | 1.5 | ... |
| −23.8 | 1 | 90°±10° | < 0.3 | 1 | ... |
| −22.0 | 4 | 70°±20° | 3.0 | 5 | ... |
| −20.5 | 3 | 80°±20° | < 1.0 | 3 | −55 |
| −19.6 | 3 | 75°±20° | 3.0 | 4 | −55 |
| −19.2 | 3 | ... | 6.5 | 8 | ... |
| −12.8 | ... | ... | ... | ... | −65 |
| +16.3 | <5 | 90°±30° | 10.0 | 10.0 | ... |
| +21.4 | 2 | ... | 3 | 5 | ... |
| Other velocities | <5 | ... | < 3 | < 6 | ... |

* Position Angle = 0° is defined as the $E$-plane in a north-south direction.

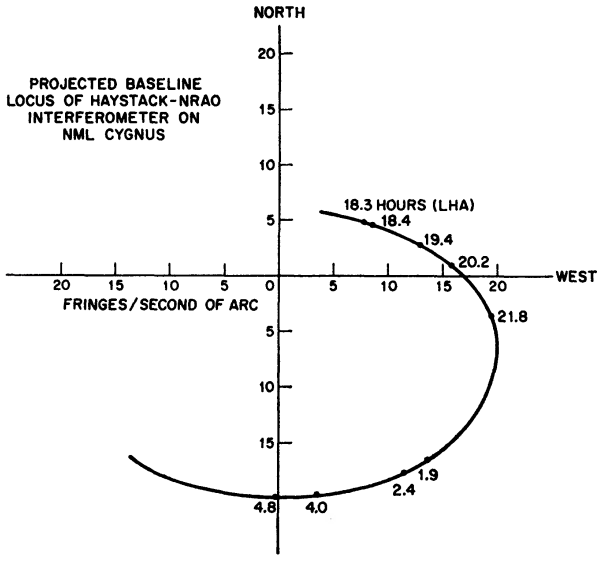


FIG. 5.—Projected baseline locus on NML Cyg obtained with the Haystack-NRAO interferometer. Measurements were obtained at the local hour angles indicated.

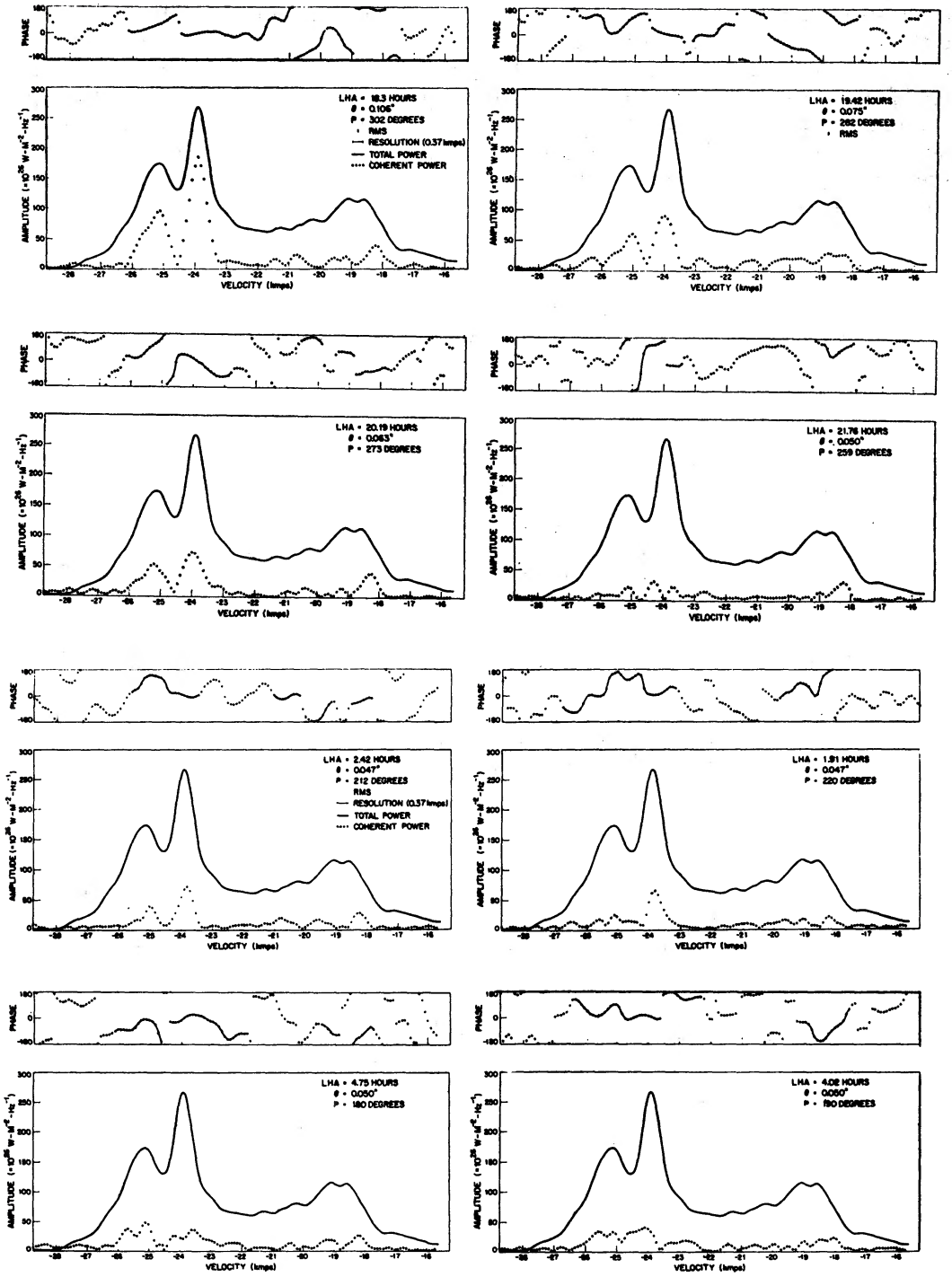


FIG. 6.—Eight visibility spectra obtained on the low-velocity features in the 1612-MHz transition in NML Cyg. Ratio of dotted spectrum to solid spectrum is the fringe amplitude. $P$ and $\theta$ are the position angle of the baseline and the effective resolution. Spectral resolution is 2.4 kHz, or 0.37 km sec$^{-1}$

A complete description of the spatial structure requires the measurement of the fringe visibility over a wide range of projected baselines. Hence, with eight projected baselines only general statements can be made about the source's structure. The structure is very complex, and there are at least fifteen spatially distinct features between $-17$ and $-27$ km sec$^{-1}$, that is, distinct peaks whose relative phases change with local hour angle. Features near $+20$ km sec$^{-1}$ were also detected and have a characteristic size of 0".08. All of the major features have the same fringe rates on a given spectrum within 2 mHz, thereby implying that they are all located within 2" of one another. Moreover, the relative fringe phases among the features change so much between spectra that it has not been possible to obtain a map of relative feature positions. The fringe amplitude at $-23.9$ km sec$^{-1}$ illustrates the complexity of the source. Because of the positions of the nulls and maxima near this velocity, this feature probably has at least three components. All that can be said with these limited data is that the characteristic feature size in the $-20$ km sec$^{-1}$ complex is $\sim$0".08 (uniform disk model). At an assumed distance of 500 pc this corresponds to a linear size of about 40 a.u. or $6 \times 10^{14}$ cm. Based on this size, the apparent brightness temperature of the strongest feature is $4 \times 10^{10}$ ° K.

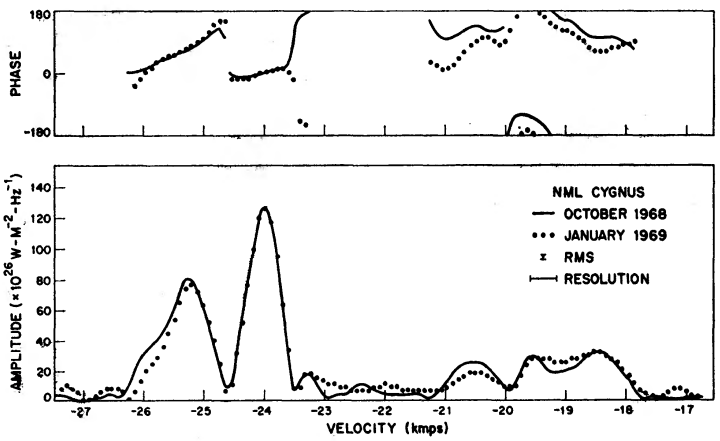


FIG. 7.—Interference spectra taken in 1968 October (*solid line*) and 1969 January (*dotted line*) on NML Cyg. Difference in local hour between measurements was 0.10 hours. Spectra have been scaled to be equal at $-23.9$ km sec$^{-1}$.

On 1969 January 13 an interference spectrum at a local hour angle of 18.5 hours was obtained and plotted over the one obtained on 1968 October 12 at 18.4 hours (see Fig. 7). The visibilities were scaled to be equal in amplitude and phase at $-23.9$ km sec$^{-1}$ for comparison purposes. The slight differences are probably attributable to the small differences in the local hour angles of observation. Hence, no changes in the apparent structure of the source of the order of 0".01 are observed over a 3-month period. During this period, the Earth moved 1.3 a.u. in the direction perpendicular to the direction of NML Cyg. There are no large changes in the apparent spatial structure of the source caused by time variations or any diffraction or focusing effect.

The absolute position of the OH source was found to be coincident with the position of the infrared source within 5". The position was measured by comparing the fringe-rate residuals of NML Cyg with those on 3C 273 over a wide range of local hour angles. The 3C 273B position was taken from the measurement by Hazard, Mackey, and Shimmins (1963), which was reported to be accurate to 0".5. From the fringe-rate residuals on 3C 273, the baseline parameters were found to be

$$D \cos \delta_B = 767.99 \text{ km}, \quad L_B = 4.73601 \text{ hours},$$

where $D$, $\delta_B$, and $L_B$ are the baseline length, declination, and local hour angle.

The position for the OH source obtained from the fringe rate residuals is $\alpha = 20^h44^m33^s.8 \pm 0^s.5$ (1950), $\delta = 39°55'56'' \pm 5''$.

The most recent accurate position for the IR star is (Hilgeman 1969) $\alpha = 20^h44^m33^s.93$ (1950), $\delta = 39°55'57''.5$.

The rms random error in the OH position determination is $\sim 1''$ in each coordinate. The error bars have been increased to account for several sources of systematic error. This result establishes the close relationship between the NML Cyg OH source and the IR star.

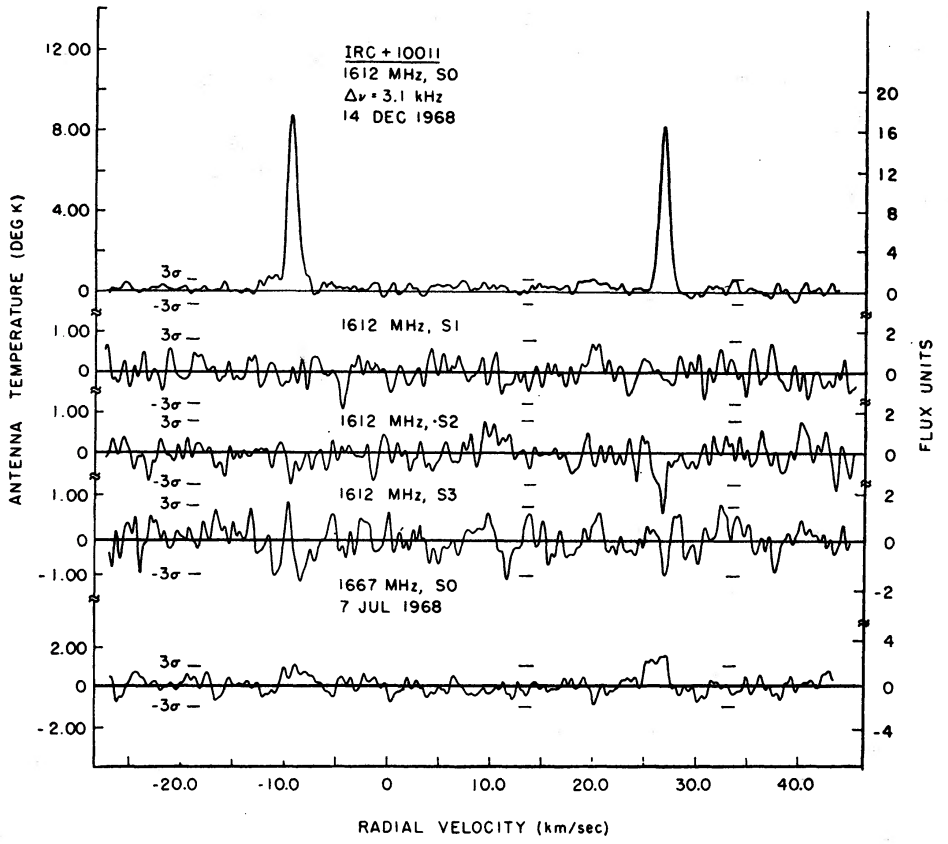


FIG. 8.—The 1612- and 1667-MHz spectra of IRC+10011 (CIT-3). $S_0$, $S_1$, $S_2$, and $S_3$ are the Stokes parameters. To convert the given LSR velocities to heliocentric velocities, add +2.4 km sec$^{-1}$.

### *b) IRC+10011*

The IR star IRC+10011 (CIT-3) was reported by Ulrich *et al.* (1966) during the CIT infrared survey. It has an *I–K* magnitude of 7.6, but no spectral type has been assigned. Wisniewski *et al.* (1967) have shown that IRC+10011 is variable in the IR.

OH emission spectra at 1612 and 1667 MHz, detected in 1968 July, are shown in Figure 8. IRC+10011 is the third strongest OH/IR source detected with a peak $S_0$ flux of 20 f.u. for each feature. This source is one of the classic examples of OH/IR emission, since its spectra have *all* the characteristics of the OH/IR emission outlined in the Introduction.

The Stokes parameters of the 1612-MHz emission are also shown in Figure 8. There is a small amount of linear polarization—~14 percent—in the 27 km sec$^{-1}$ feature. There is also a hint of some circular polarization in the −9 km sec$^{-1}$ feature that changes from right- to left-circular across the feature, suggestive of Zeeman splitting. The 1667-MHz emission was found to have less than 25 percent circular polarization.

The position of the OH emission was found to be coincident with the IR star to within 5′.

A high-resolution spectrum of the 1612-MHz emission, shown in Figure 9, reveals that each of the main features is composed of three to four separate narrow features with typical half-power widths of about 0.6 km sec$^{-1}$ or 3 kHz. The fact that each of the main features is composed of three to four separate features could explain the polarization variation across the features; for example, the separate features could each have some characteristic polarization.

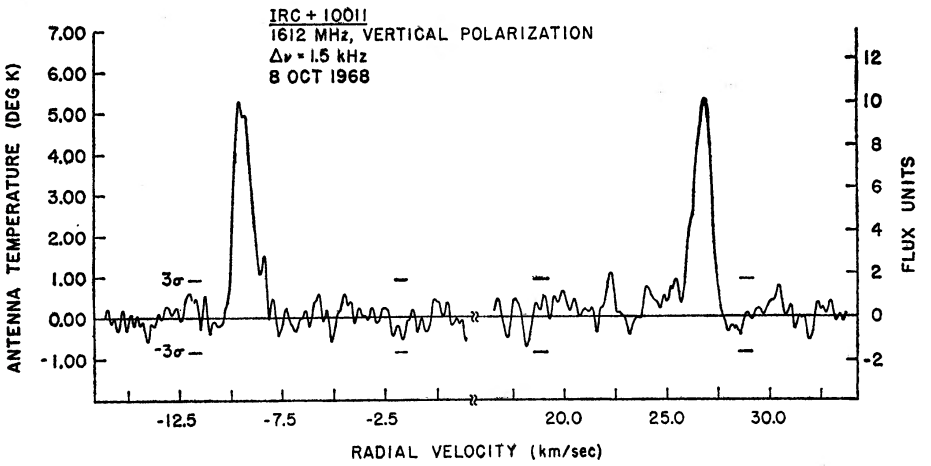


FIG. 9.—High-resolution 1612-MHz spectrum of IRC+10011

TABLE 4

TIME VARIATIONS OF IRC+10011*

| DATE | −9 KM SEC$^{-1}$ FEATURE | | +27 KM SEC$^{-1}$ FEATURE | | TOTAL |
|---|---|---|---|---|---|
| | $S_0$ Peak (f.u.) | $\int S_0 dv$ (W m$^{-2}$×10$^{-23}$) | $S_0$ Peak (f.u.) | $\int S_0 dv$ (W m$^{-2}$×10$^{-23}$) | $\int S_0 dv$ (W m$^{-2}$×10$^{-23}$) |
| 1968 July 11..... | 21 | 145 | 21.5 | 135 | 280 |
| 1968 December 14..... | 17.2 | 129 | 16.4 | 103 | 232 |

* Relative errors are ±5 percent.

The source is variable in the IR, and the OH emission has also been found to be variable. Table 4 summarizes these data. The total flux decreased by 17 percent. The individual features also decreased but seemed to do so at slightly different rates. During this period the IR flux decreased (Neugebauer 1969), suggesting that the OH and IR fluxes are correlated.

### c) *NML Taurus*

NML Taurus is a Mira-type variable with a period greater than 532 days. It has been classified as an M8e spectral type (Wing, Spinrad, and Kuhi 1967). OH emission spectra, first detected from NML Tau in 1968 June at frequencies of 1612 and 1667 MHz, are shown in Figure 10. Two emission features at 1612 MHz occur at 17.4 and 50.4 km sec$^{-1}$ and are of nearly equal strength, 2.4 f.u. The emission feature at 1667 MHz also has a strength of approximately 2.4 f.u., but its velocity is 15 km sec$^{-1}$, 2.5 km sec$^{-1}$

lower than the corresponding 1612-MHz feature, suggesting that this emission may originate from a different spatial location in the source. No circular polarization at either 1612 or 1667 MHz greater than 25 percent was detected.

It is interesting to note that the radial velocity (with respect to the local standard of rest) of the optical absorption feature is 51 ± 5 km sec$^{-1}$ (Wing *et al.* 1967) and the velocity of one of the 1612-MHz features is 50.4 km sec$^{-1}$. Wing *et al.* (1967) also measured a velocity of 31 km sec$^{-1}$ for the hydrogen emission line Pλ.

In 1968 December additional spectra were obtained on NML Tau which showed definite changes from the June data (a time difference of 168 days). For example, when linear polarization at 1612 MHz was used, the 17 km sec$^{-1}$ feature was not detectable with an upper limit of 0.4 f.u. while the +50 km sec$^{-1}$ feature had a peak flux of 1 f.u., consistent with the July observations. In December, at 1667 MHz the 15 km sec$^{-1}$ feature was not detected with an upper limit of 0.6 f.u. when linear polarization was

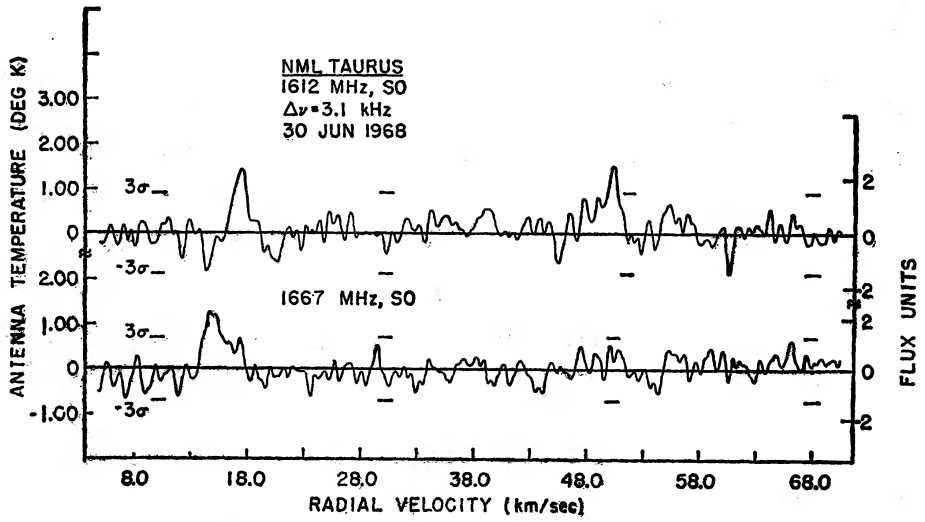


FIG. 10.—The 1612- and 1667-MHz $S_0$ spectra of NML Tau. To convert the given LSR velocities to heliocentric velocities, add +12.3 km sec$^{-1}$.

used. There are two possibilities for this variation: either the features vary in time or they are linearly polarized. Our observations of other IR sources show very little polarization, and since NML Tau is known to be a Mira-type variable in which the IR flux decreased from July to December (Neugebauer 1969), time variations seem to be the most probable explanation.

### *d) IRC+50137*

OH emission at 1612 MHz as detected from IRC+50137 in 1968 December is shown in Figure 11. A tentative detection of a 1667-MHz feature at −6 km sec$^{-1}$ was established. No circular polarization was detected with limits of 10 percent for the 19 km sec$^{-1}$ feature and 40 percent for the −13 km sec$^{-1}$ emission. There is an indication that the OH flux decreased in 1968 from October to December; however, this was not verified because of system uncertainties.

### *e) IRC−20197*

Only 1612-MHz emission has been detected from IRC−20197; the spectrum is shown in Figure 12. No circular polarization was detected in the 1612-MHz emission with an

upper limit of 30 percent, and no time variations of the emission were noted in 1968 between October and December.

*f) IRC+20281*

The IR star IRC+20281 (CIT-7) was first reported in 1966 during the CIT infrared survey (Ulrich *et al.* 1966), and it was identified with the variable star WX Ser. This star is a Mira-type variable with a period of 425 days and has been classified as a M8.5e type (Wisniewski *et al.* 1967). IRC+20281 is also a variable in the IR.

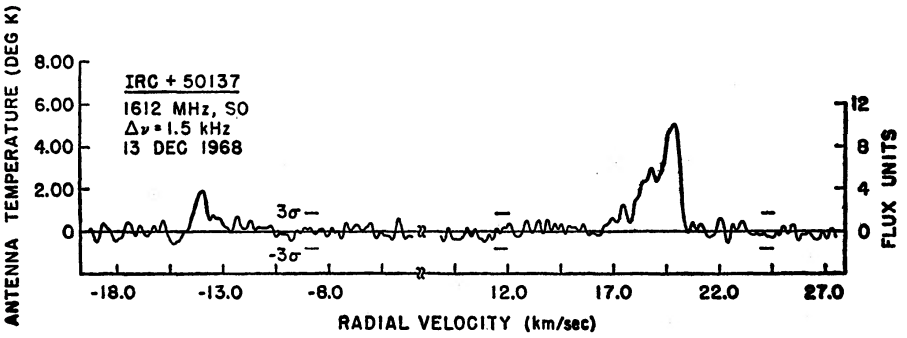


FIG. 11.—The 1612-MHz $S_0$ spectrum of IRC+50137. To convert the given LSR velocities to heliocentric velocities, add +2.2 km sec$^{-1}$.

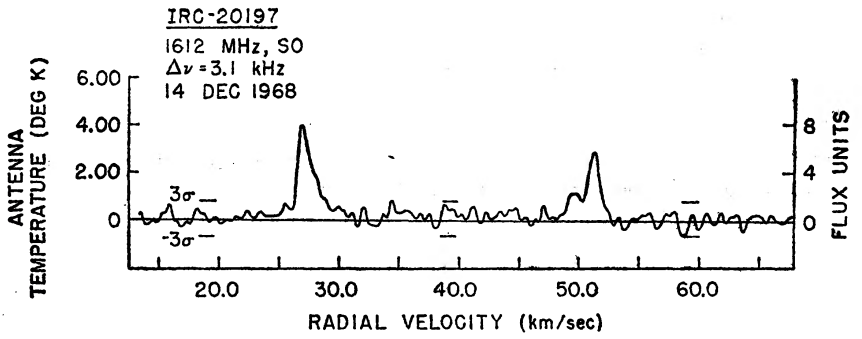


FIG. 12.—The 1612-MHz $S_0$ spectrum of IRC−20197. To convert the given LSR velocities to heliocentric velocities, add +12.9 km sec$^{-1}$.

OH emission spectra, detected in 1968 July at 1612, 1665, and 1667 MHz, are shown in Figure 13. The 1612-MHz emission occurs at velocities of −0.5 and 13.2 km sec$^{-1}$ and has less than 25 percent circular polarization. The 1665- and 1667-MHz emission only occur at the −0.5 and −1.0 km sec$^{-1}$ velocities and have less than 20 percent and 40 percent circular polarization, respectively. The fact that the 1667-MHz velocity is slightly lower may indicate that this emission is coming from a slightly different location. No time variations were observed in 1968 between July and December.

*g) IRC+10406*

IRC+10406 has been identified with the Mira variable R Aql, spectral type M7e with an $I$–$K$ magnitude of 5.0. IRC+10406 is the second strongest of the OH/IR sources detected, with a 1612-MHz peak flux of 72 f.u. at 53.8 km sec$^{-1}$. The emission at 1667 MHz is weaker (2 f.u.) and occurs at a velocity of 43 km sec$^{-1}$. The 1612-MHz

spectrum is shown in Figure 14. The 1612-MHz emission at 53.8 km sec$^{-1}$ appears to consist of one feature with an equivalent half-width of 1 km sec$^{-1}$, corresponding to a kinetic temperature of 360° K. The main 1612-MHz emission at 53.8 km sec$^{-1}$ has less than 6 percent circular polarization, and the weaker line at 43 km sec$^{-1}$ has less than 30 percent circular polarization. There was an indication of a decrease in the OH flux from IRC+10406 during the period in 1968 from October to December; however, this cannot be confirmed because of uncertainties in the system calibrations.

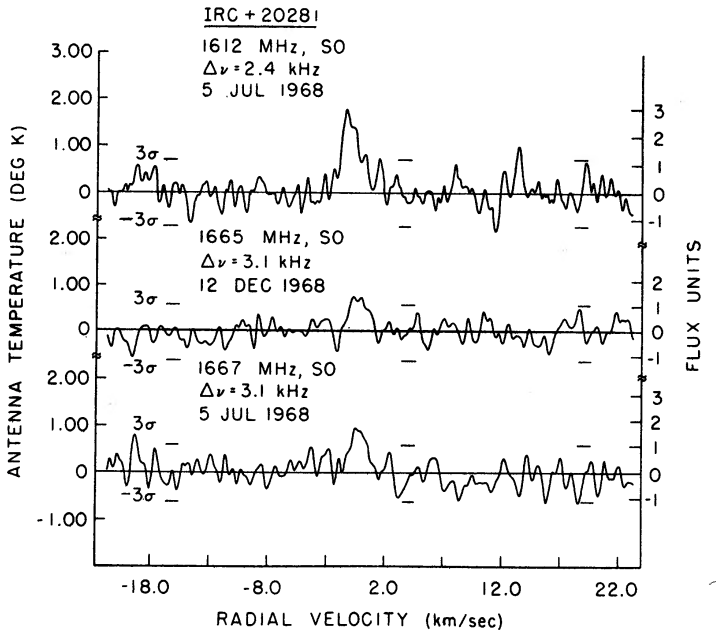


FIG. 13.—The 1612-, 1665-, and 1667-MHz $S_0$ spectra of IRC+20281 (WX Ser, CIT-7). To convert the given LSR velocities to heliocentric velocities, add −16.0 km sec$^{-1}$.

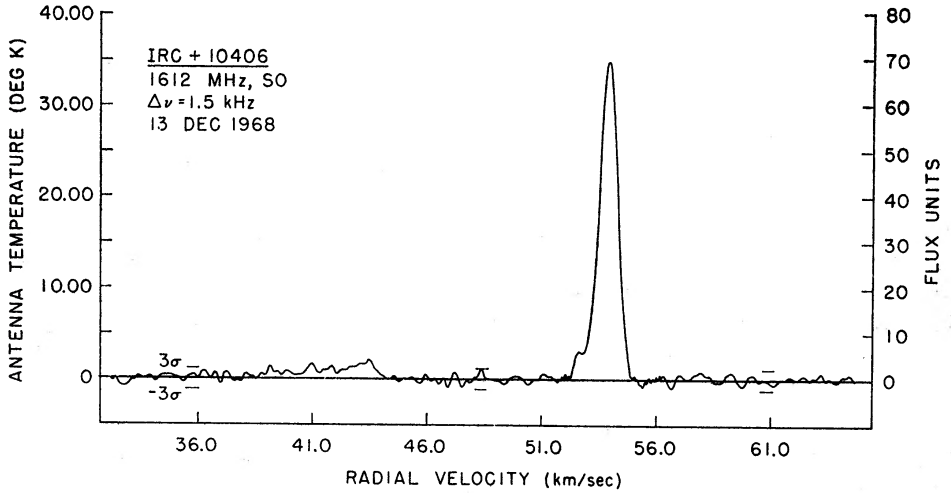


FIG. 14.—The 1612-MHz $S_0$ spectrum of IRC+10406 (R Aql). To convert the given LSR velocities to heliocentric velocities, add −17.9 km sec$^{-1}$.

*h) Observations with Negative Results*

All of the sources observed in which OH was not detected are listed in Tables 5, 6, and 7 with a brief summary of the observations. There were fifty-three IR stars, eight well-known red giants, and seven T Tauri stars in which there was no detectable OH.

There are several possible explanations for the fact that only 12 percent of the IR stars have detectable OH associated with them. First, many of the IR stars could have OH emission below the threshold of detectability, because of intrinsic strength, distance, or a beaming of the maser. Since some of the IR stars are variables, the observations reported here could have been made during a minimum of the IR flux, and thus the OH emission, if correlated, may have been too weak to detect. Second, some of the IR stars may not have sufficient IR flux to pump the required OH maser. Third, some of the IR stars may be of the wrong type for OH emission—for example, carbon stars in which the abundance of OH might possibly be too small. Finally, the conditions for OH emission may be favorable for only a limited time in the evolution of the star.

TABLE 5

INFRARED STARS WITHOUT OH EMISSION

| Source | Observation Notes | Remarks | Source | Observation Notes | Remarks |
|---|---|---|---|---|---|
| IRC+40004 | 1 | CIT-1 | IRC+20328 | 1 | MW Her, CIT-9 |
| IRC−30002 | 2,3 | SY Scl | IRC−30308 | 2 | |
| IRC+70008 | 2 | | IRC−10381 | 2 | |
| IRC+30015 | 1 | CIT-2 | IRC−20418 | 3 | |
| IRC+50030 | 2,3 | | IRC−10395 | 2 | |
| IRC+30021 | 2 | | IRC−10396 | 2 | |
| IRC+60092 | 1 | CIT-4 | IRC+00379 | 2 | Near W43 |
| IRC+50096 | 1 | CIT-5 | IRC+00387 | 2 | |
| IRC+40070 | 2 | | IRC+00396 | 2,3 | Near W44 |
| IRC+20085 | 2 | | IRC−30398 | 2 | |
| IRC+50122 | 2 | | IRC+20404 | 2 | |
| IRC+60144 | 2 | | IRC+40413 | 2 | |
| IRC+50130 | 2 | AU Aur | IRC+40431 | 2 | |
| IRC+30114 | 2 | S Aur | IRC+40432 | 1 | CIT-10 |
| IRC+40135 | 2 | RU Aur | IRC+40434 | 2 | |
| IRC+70066 | 2 | | IRC+40439 | 1 | CIT-11 |
| IRC+70067 | 2 | V Cam | IRC+40442 | 1 | DG Cyg, CIT-12 |
| IRC+00102 | 2 | | IRC+50346 | 2 | DS Cyg |
| IRC+40156 | 2,3 | | IRC+50357 | 2 | |
| IRC+60169 | 2 | | IRC+50362 | 2 | |
| IRC−20131 | 2 | | IRC+40483 | 2 | |
| IRC+30219 | 1 | CIT-6 | IRC+40485 | 1 | CIT-13 |
| IRC+30283 | 1 | RU Her, CIT-8 | IRC+60377 | 2 | |
| IRC−10355 | 2 | | IRC+10525 | 2 | |
| IRC−30301 | 2 | | IRC+40540 | 2 | |
| IRC−20368 | 2 | | IRC+40545 | 1 | CIT-14 |
| IRC−30303 | 2 | | | | |

OBSERVATION NOTES

1. Observed in 1968 July at all four OH frequencies over a velocity range of ±90 km sec$^{-1}$ with a resolution bandwidth of 3.1 kHz. The $S_0$ flux was less than 2 f.u.
2. Observed in 1968 October at 1612 MHz over a velocity range of ±95 km sec$^{-1}$ with a resolution bandwidth of 3.1 kHz. The flux measured with a vertically polarized feed was less than 2 f.u.
3. Observed in 1968 December at 1612 MHz over a velocity range of ±200 km sec$^{-1}$ with a resolution bandwidth of 3.9 kHz. The flux measured with a linearly polarized feed ($E$-plane north-south) was less than 2 f.u.

The list of red-giant stars includes many well-known stars. The negative result for Mira (*o* Ceti) is of special interest because this is the prototype for at least six of the OH/IR sources. This suggests that Mira might have OH emission. It will be necessary to try to detect OH emission at selected points in Mira's light cycle before a definite result is established, but it should be noted that the 1968 October observations corresponded to the time of maximum brightness in Mira's light curve.

There are two special cases of interest among the T Tauri stars. First, special emphasis was placed on the source R Mon, since it is a strong IR source and is generally believed to be a preplanetary system composed of dense clouds (Herbig 1968). No OH emission

TABLE 6

RED-GIANT STARS WITHOUT OH EMISSION

| Source | Observation Notes* | Remarks |
|---|---|---|
| R And | 2 | S6e(M7e) |
| *o* Cet | 2 | M6e, IRC+00030 |
| TX Cam | 1 | M9, IRC+60150 |
| α Ori | 2 | M2 I |
| α Sco | 1 | M1 Ib |
| χ Cyg | 2 | M6, IRC+30395 |
| μ Cep | 2 | M2e Ia |
| BS 8421 | 2 | M8 |

* Refer to Table 5 for observation notes.

TABLE 7

T TAURI STARS WITHOUT OH EMISSION

| Source | Observation Notes* | Remarks |
|---|---|---|
| RY Tau | 1 | G0e |
| T Tau | 1 | G5e |
| RW Aur | 2 | G5e |
| GW Ori | 2,3 | K3e |
| V380 Ori | 2 | A2 |
| FU Ori | 2,3 | F5 |
| R Mon | 1,2 | K1 |

* Refer to Table 5 for observation notes.

was detected at 1612, 1665, or 1667 MHz to a limit of 1 f.u. or at 1720 MHz to a limit of 2 f.u. The other special case is the star FU Ori, which is the star that "turned on" in 1939 (Herbig 1966) and thus is known to be a very young star. No OH emission was detected at 1612 MHz to a lower limit of 4 f.u. The negative results obtained for these young stars may place limits on the conditions under which we can expect to observe OH emission, a possibility which suggests that young stars may not provide the necessary conditions for the IR-pumped OH maser (see § IV*a*).

## IV. DISCUSSION

### *a) Near-infrared Pumping Model*

One of the unique characteristics of these OH/IR sources is the distribution of emission among the four OH frequencies. A summary of the emission at each frequency in

terms of the integrated flux is presented in Table 8. Five conclusions can be reached from these data:

1. The 1612-MHz emission is the strongest by factors of 2 to 100 compared with the other emission frequencies.
2. There is no preference for the strongest 1612-MHz emission to occur at either the low or the high velocities.
3. In all cases in which good sensitivity limits have been established, weak 1667-MHz emission accompanies the 1612-MHz emission. This may imply that weak 1667-MHz emission always occurs with the 1612-MHz emission. The 1667-MHz emission does not seem to favor either the stronger or the weaker 1612-MHz emission velocity.
4. When 1667-MHz emission is present, 1665-MHz emission may occur.
5. Emission never occurs at 1720 MHz.

These characteristics of the OH/IR emission define a separate class of OH sources, and Turner (1967, 1969) has classified this type of OH source as the class II-b type (1612-MHz emission strongest). These characteristics noted in the OH/IR sources served to define more precisely the properties of the class II-b sources.

TABLE 8

VALUES OF INTEGRATED FLUX $\int S_0 dv$ (W $m^{-2} \times 10^{-22}$*)

| Source | 1612 MHz | | 1665 MHz | | 1667 MHz | | 1720 MHz |
|---|---|---|---|---|---|---|---|
| | Low Vel. | High Vel. | Low Vel. | High Vel. | Low Vel. | High Vel. | |
| NML Cyg | 1250 | 410 | 5.0 | † | ... | 9.6 | ... |
| IRC+10011 | 14.0 | 14.0 | ... | ... | 2.0 | 3.1 | ... |
| NML Tau | 2.2 | 2.8 | ... | ... | 2.5 | ... | ... |
| IRC+50137 | 2.2 | 8.6 | ... | ... | ... | † | ... |
| IRC−20197 | 8.5 | 5.0 | ‡ | ‡ | ‡ | ‡ | ... |
| IRC+20281 | 3.0 | 0.7 | 1.4 | ... | 1.7 | ... | ... |
| IRC+10406 | 5.6 | 38.4 | ... | ... | 5 | ... | ... |

NOTE.—No entry implies no emission greater than 1 f.u.
* Absolute errors are ± 25 percent.
† Possible feature.
‡ No detection greater than 5 f.u.

The only detailed theory which predicts many of the observed properties is the theory of IR pumping of interstellar OH (Litvak 1969*a*). In this section the main predictions of this theory will be compared with the observed facts and a calculation of the required source conditions will be made.

The theory of IR pumping predicts that emission in the 1612-MHz satellite line will be strongest if there is strong 2.8-$\mu$ IR radiation and the OH clouds have a large optical depth to provide for resonance trapping of the far-IR photons. The 2.8-$\mu$ radiation will excite the OH molecules from the ground state to the first vibrational state where they will eventually cascade down and, in conjunction with resonance trapping, invert the populations of the 1612-MHz transition. A blackbody at a temperature of 1000° K has the peak of its radiation near 2.8 $\mu$ and has an $I-K$ magnitude of 7. The observed OH/IR sources have $I-K$ magnitudes close to 7, and thus the requirement for strong near-IR radiation is satisfied. The condition for strong near-IR radiation does not rule out OH emission associated with sources whose effective temperatures are greater than 1000° K, since the OH molecules could be located in regions of cooler temperatures.

The theory of near-IR pumping also predicts that the 1720-MHz transition will be anti-inverted. This is in agreement with the observations of no 1720-MHz emission. Weak main-line emission is observed in most cases, and this is predicted by the theory when the kinetic temperature of the OH is greater than 440° K.

If the OH molecules are pumped by 2.8-$\mu$ radiation, one would expect to observe the absorption of 2.8-$\mu$ IR radiation in the OH/IR sources. This is a difficult observation, however, because of atmospheric absorption and because the expected line width $\Delta\lambda = (\Delta\nu/\nu)\lambda \sim 10^{-5}\ \mu$ is extremely small. One of the highest-resolution IR spectrometers in use today has a resolution of $10^{-4}\ \mu$ (8 cm$^{-1}$) (Johnson 1968).

The theory of near-IR pumping requires that the density of the region be low to insure that the collision rate be much less than the IR-pumping rate. This condition can be expressed as

$$\frac{B_{12}I_{\rm IR}\Omega_r}{R_{\rm coll}} = \frac{5 \times 10^{15}\, I_{\rm IR}\Omega_{\rm IR}}{N_{\rm H}} \geq 10\,, \tag{1}$$

where $B_{12}$ = Einstein $B$ absorption coefficient for the 2.8 transition, $I_{\rm IR}$ = IR source intensity at the OH cloud, $\Omega_{\rm IR}$ = solid angle subtended by the OH cloud at the source, $R_{\rm coll}$ = collision rate caused by hydrogen atoms = $4 \times 10^{-10}\, N_{\rm H}$ sec$^{-1}$ (Rogers and Barrett 1968), and $N_{\rm H}$ = number of hydrogen atoms per cm$^3$.

If the IR source of temperature 1000° K subtends a solid angle of 1 sterad at the OH cloud (Litvak 1969*a*), the pump flux $I_{\rm IR}\Omega_{\rm IR} = 10^{-7}$ erg cm$^{-2}$ sec$^{-1}$ Hz$^{-1}$, and thus $N_{\rm H} \leq 5 \times 10^7$ cm$^{-3}$, or a density of $\rho \leq 5 \times 10^{-17}$ g cm$^{-3}$.

The theory of IR pumping requires large optical depths in the IR to obtain the 1612-MHz emission. For the cases considered by Litvak (1969), the requirement was that $N_{\rm OH}l_0 \approx 10^{17}$ cm$^{-2}$, where $N_{\rm OH}$ is the number of OH molecules per cm$^3$ and $l_0$ is the length of the cloud. The assumption $N_{\rm OH} \sim 10^{-6}N_{\rm H}$ puts a lower limit on the cloud length of $l_0 > 2 \times 10^{15}$ cm $\approx$ 100 a.u.

To summarize, it appears that the observed characteristics of the microwave radiation from the OH/IR sources can be explained by the theory of IR pumping. The temperature, density, and dimensions predicted from this theory are conditions that must be met in the regions near the cool sources where the OH emission is observed. Power requirements will be considered in § IV*c*.

A further observation that supports the theory of IR pumping of the OH maser is that the time variations of the OH seem to be correlated with the IR time variations. In the two cases in which the OH has been observed to decrease, IRC+10011 and NML Tau, the IR flux has also decreased (Neugebauer 1969). In the case of NML Cyg, both the OH and IR emission were constant over the 6-month period of observations.

### *b) Maser Models*

When weak main-line emission occurs, the theory of near-IR pumping predicts that the OH molecules will be located in a hot or a turbulent region. Litvak (1969*a*) has calculated that, for large optical depths, $N_{\rm OH}l_0 \geq 10^{17}$ cm$^{-2}$, and kinetic temperatures $T_K \geq 440°$ K, the excited-state IR absorption lines (to the $^2\pi_{1/2}, J = \frac{3}{2}$ and $J = \frac{5}{2}$ states) would be expected to be overlapped in the lower $\Lambda$ doublets, and emission would be observed at 1667 MHz and possibly at 1665 MHz. As noted, weak 1667-MHz emission usually occurs with the strong 1612-MHz emission, thereby implying that the OH molecules have kinetic temperatures of at least 440° K.

A summary of the estimated line widths for individual features and the kinetic temperatures calculated from these line widths for each of the sources is presented in Table 9. The radial velocities of the emission with respect to the local standard of rest are listed in column (2), and in column (3) the heliocentric velocities are listed. In these calculations, turbulent broadening was neglected. The kinetic temperatures range from 100° to 500° K, and thus, if the kinetic temperature is required to be greater than 440° K, it seems that the emission lines have been narrowed by factors of 1 to 2.

In an unsaturated maser, where the excitation rate for OH molecules exceeds the excitation rate with microwave photons, the received flux is proportional to

$$S \sim e^{\tau_\nu}\,, \tag{2}$$

where $\tau_\nu = hB_{21}g_2(\nu/\Delta\nu)\int ndl$, $B_{21}$ = Einstein $B$ coefficient for stimulated microwave emission, $g_2$ = degeneracy of the upper state, $\nu/\Delta\nu$ = ratio of line frequency to bandwidth of feature $\approx 4 \times 10^{+5}$, and $\int l\Delta ndl = \int (n_2/g_2 - n_1/g_1)dl$ = population inversion integrated along the path length $l$. For $\tau_\nu \geq 4$ the observed Doppler-broadened emission lines will have been narrowed by approximately $\sqrt{\tau_\nu}$, because of the large amplification at the line center. Therefore, when the lines seem to be narrowed by factors of 1 to 2, this would indicate that $\tau_\nu$ was less than 4. To explain the observed brightness temperature of NML Cyg of $T_b \sim 10^{10}$ K (§ III*a*), the value of $\tau_\nu$ must be between 16 and 23 in the case of an unsaturated maser, depending on the input temperature of the maser. This would predict line narrowing by a factor of 4–5, which is in conflict with the value of 1–2 predicted by the theory of IR pumping. Also, this large value of $\tau$ would imply kinetic temperatures of 1600°–10000° K, which seem to be high for the regions in which the OH masering cloud is located in these sources.

TABLE 9

1612-MHz VELOCITIES, LINE WIDTHS, AND KINETIC TEMPERATURES

| Source (1) | Velocity of Emission (km sec$^{-1}$) LSR (2) | Heliocentric (3) | No. of Individual Features (4) | Estimated Line Widths* (km sec$^{-1}$) (5) | Equivalent Kinetic Temperatures† (° K) (6) |
|---|---|---|---|---|---|
| NML Cyg..... | −22 | −38.5 | >20 | 0.5–0.9 | 90–300 |
| | +20 | + 3.5 | >20 | | |
| IRC+10011..... | − 9 | − 6.6 | 3–4 | 0.5–0.8 | 90–240 |
| | +27 | +29.4 | 3–4 | | |
| NML Tau..... | +17 | +29.3 | 2 | 0.8–1.0 | 240–360 |
| | +50 | +62.3 | 3 | | |
| IRC+50137..... | −14 | −11.8 | 2 | 0.7–1.0 | 180–360 |
| | +19 | +21.2 | 5–6 | | |
| IRC−20197..... | +27 | +39.9 | 3 | 0.9–1.2 | 300–520 |
| | +51 | +63.9 | 3 | | |
| IRC+20281..... | − 0.5 | −16.5 | 4 | 0.7–0.9 | 180–300 |
| | +13.2 | − 2.8 | 1–2 | | |
| IRC+10406..... | +43 | +25.1 | 2 | 0.8–1.0 | 240–360 |
| | +54 | +36.1 | 2 | | |

* Instrumental broadening removed.

† The kinetic temperatures have not been corrected for any turbulent broadening.

In a fully saturated maser in which the output is limited by the number of excited OH molecules, the received flux is proportional to

$$S_\nu \sim \tau_\nu , \tag{3}$$

and no line narrowing is predicted. Since some line narrowing is necessary, based on the results of the theory of IR pumping, it is proposed that the OH/IR masers are *partially saturated*. Litvak (1969*b*) has shown that the emission lines would be narrowed by a factor of 1.5 if the length of the maser were twice the length of the maser when it first became saturated. This is approximately the case that best fits the observed line narrowing.

The observed fact that the strengths of the individual emission features in the OH/IR sources are within 2 orders of magnitude of each other is also an argument in favor of the partially saturated maser because in this case the flux is proportional to $\tau_\nu$. With an unsaturated maser, to keep the features within a factor of 100, $\tau_\nu$ would have to vary by less than 25 percent from cloud to cloud, which seems unlikely.

A further argument for the saturated maser concerns the polarization of the signals. In this case, the main lines could have significant circular polarization (Heer and Settles 1967), as observed in NML Cyg at 1665 MHz, which could influence the polarization at 1612 MHz, a situation which is also observed in NML Cyg. No circular polarization of the 1667-MHz emission is evident from the observations, within the limits of $\pm 25$ percent.

There are two additional observations that may be made to test the conclusion that the maser is saturated. The first is the search for emission from the isotope $O^{18}H$ in the OH/IR sources. If both the $O^{16}H$ maser and the $O^{18}H$ maser are saturated, the difference in the received fluxes would be proportional to their abundance ratios. On Earth the oxygen abundance ratio is $O^{16}/O^{18} \simeq 500$, and if the $O^{18}H$ emission were down by a factor of 500, it would still be detectable. If the $O^{18}H$ maser is not saturated, then emission could be reduced by anywhere from 1/500 to the 1/500th power, and this would be undetectable. Hence, if the $O^{16}H$ maser has just become saturated, then the $O^{18}H$ maser would be unsaturated and would be undetectable.

TABLE 10

MICROWAVE PUMPING RATES FOR OH/IR SOURCES

| Source (1) | Galactic Model Distance (pc) (2) | Estimated* Distances (pc) (3) | Integrated Flux $\int S_0 dv$ ($10^{-22}$ W m$^{-2}$) (4) | Microwave Photon Rate $R_m$† ($10^{42}$ sec$^{-1}$) (5) |
|---|---|---|---|---|
| NML Cyg..... | 0, 3600 | 500 | 1675 | 440.0 |
| IRC+10011..... | ‡ | 330 | 33 | 3.8 |
| NML Tau..... | ‡ | 500 | 8 | 2.1 |
| IRC+50137..... | ‡ | 1800 | 11 | 40.0 |
| IRC−20197..... | 3900 | 700 | 14 | 6.5 |
| IRC+20281..... | 800, 17000 | 330 | 7 | 0.85 |
| IRC+10406..... | 3500, 11000 | ... | 49 | 630.0 |

* See text. † Into $4\pi$ steradians. ‡ No distance possible.

The relationship between the time variations of the OH emission and the IR emission can also be measured. It is expected that the saturated maser would be much less sensitive than the unsaturated maser to changes in the IR intensity, and thus measurements of this correlation could provide a clue as to the type of masering process.

### c) *Power Considerations*

The total power per square meter received from the OH/IR source is

$$P_{\text{rec}} = \int S_\nu d\nu = \frac{h\nu R_m}{D^2 \Omega_m} \text{ watts m}^{-2}, \tag{4}$$

where $S_\nu$ = received flux density (W m$^{-2}$ Hz$^{-1}$), $D$ = source distance ($m$), $\Omega_m$ = solid angle (steradians) of microwave maser emission, and $R_m$ = rate of microwave photons sec$^{-1}$.

The total power received has been measured in the observations, and the distance $D$ can be estimated to derive a value for $R_m$, under the assumption of isotropic emission ($\Omega_m = 4\pi$). The results of these calculations are presented in Table 10.

The distances were estimated first by using the median velocity of emission and the Schmidt model of galactic rotation. The results of these calculations are shown in Table 10, column (2). If these stars are old and have moved great distances from where they

were formed, it might be expected that the galactic-model distances would have little meaning. This seems to be the case, as these distances imply much too large luminosities for the IR stars. Thus, it is necessary to use another method for determining the distances. Five of these sources have galactic latitudes greater than 7°, which places a limit on their distances if it is assumed that they are in the galactic disk. The distances of these sources (Table 10, col. [3]) were taken as the distance between the Sun and the edge of the disk in the direction of the source, under the assumption of a galactic-disk thickness for gM type stars of 500 pc (Plaut 1965). The distance to NML Cyg was chosen to be 500 pc based on arguments of the IR polarization (Johnson 1968).

The large distance for IRC+10406 makes this source the strongest of the OH/IR sources by 1 order of magnitude. This distance may be too large by a factor of 3–10; however, until further statistics on the nature of the OH/IR sources are available, it is not reasonable to assume any other values for this distance. Once the total received IR flux is measured from this star, it may be possible to place limits on its distance based on considerations of absolute luminosity.

The rate of microwave photons can be calculated from the theory of Litvak (1969*a*). For a saturated masering cloud of OH the rate of microwave photons is

$$R_m = W_s \int \Delta n_0 dv \text{ photons sec}^{-1} , \tag{5}$$

where $W_s$ = saturation-rate parameter, which is a function of the various exciting rates of the lambda doublet; $\Delta n_0 = (n_2/g_2 - n_1/g_1)_0$ = unsaturated population inversion; and $v$ = volume of the OH cloud. Now, in the case of near-IR pumping by a 1000° K blackbody source which subtends a solid angle of 1 sterad at the OH cloud, the IR-pumping rate at the front of the cloud will be $R_{IR} = 10^{-1}$ sec$^{-1}$ (Litvak 1969*a*). In § IV*a* this led to the condition for the density and the cloud length. For these conditions $W_s = 6 \times 10^{-3}$ sec$^{-1}$ and $\int \Delta n_0 dl = 5 \times 10^{14}$ photons cm$^{-2}$, values which give

$$R_m = 3 \times 10^{12} A \text{ photons sec}^{-1} , \tag{6}$$

where $A$ is the cloud area. If the solid angle of microwave emission is determined by the geometry of the source, $\Omega_m = A l_0^{-2}$, and if isotropic emission is assumed when all the individual features are considered, then

$$R_m = 3.8 \times 10^{13} l_0^2 = 1.5 \times 10^{44} \text{ photons sec}^{-1} . \tag{7}$$

The derived photon rate for NML Cyg, under an assumed distance of 500 pc, is $4.4 \times 10^{44}$ photons sec$^{-1}$, only a factor of 3 greater than this rough theoretical calculation. It is clear that the near-IR pumping model can supply a sufficient amount of energy to explain the observed emission from all of the OH/IR sources.

### *d) Geometric Model*

As noted in §§ I and II, the OH emission from the OH/IR sources is concentrated in two main ranges of velocity. This characteristic is suggestive of a model for the source in which the OH clouds are contracting, expanding, and/or rotating about the IR source. Because of the basic differences between a contracting (or expanding) and a rotating motion, it should be possible to obtain measurements to distinguish between the two types of motion. It is also possible to distinguish between the rotating, contracting, and expanding models from physical arguments. The following discussion will briefly illustrate the two basic models, point out their differences, and suggest observational tests to distinguish between them. The simplified configuration that will be considered is that of a spherical distribution of clouds around the IR source, where at some radius the temperatures and densities are in the correct range required for the IR pumping of the OH maser.

The first model to be considered is one in which the clouds of material are rotating around a central source. The advantage of this model is that it is possible to obtain long path lengths at nearly constant velocity if the clouds are at a constant radius from the star. If one OH cloud subtends a solid angle of 1 sterad at the center of the IR source, then the length of the cloud could be of the order of the radial distance to the OH cloud. Because of the gravitational force, the resulting stable configuration would have the OH clouds concentrated in the disk. The emission would be confined to two main ranges of velocity coming from each side of the disk, a prediction that is in agreement with the observations. The multiple features would arise from the multiple clouds. Because of the rotation of the source, it would be expected that the emission features would change their velocity on the time scale of the rotational period. If a radius of $10^{15}$ cm and a rotational velocity of $2 \times 10^6$ cm sec$^{-1}$ (typical observed value) are assumed, this period would be approximately 20 years. Small changes in velocity should be noted in a small fraction of this time. Since no change in the radial velocity of the individual features of NML Cyg or IRC+10011 was observed over a 6-month span, this observation argues against the rotational model.

The rotating model requires a large amount of angular momentum. If a uniform-density disk with a radius of $10^{14}$ cm with 1 $\mathfrak{M}_\odot$ is assumed to be rotating at $2 \times 10^6$ cm sec$^{-1}$, the total angular momentum would be

$$L = \tfrac{1}{2}mvr = 2 \times 10^{53} \text{ g cm}^{-2} \text{ sec}^{-1} . \quad (8)$$

This is a factor of $10^3$ times the total angular momentum of the solar system and thus makes the rotating model unlikely.

Another model is that of the contracting or expanding spherical cloud. Contraction could be due to gravitational collapse, while expansion could be due to a shock wave or stellar wind from the source. In the simple case of pure gravitational contraction (with internal pressure neglected) the required velocities of approximately 10 km sec$^{-1}$ can be realized. The problem with this model, however, is that the OH cloud must be at very large distances from the center to obtain the required path lengths of $2 \times 10^{15}$ cm with the necessary small velocity gradients at this distance. The OH cloud would subtend a solid angle of only $2 \times 10^{-3}$ sterad from the IR star, which would be inadequate for the IR pumping of the OH maser. Larson (1968) has calculated the radial velocity as a function of radius for a much more sophisticated collapsing-protostar model, and his results show that it is not possible to obtain path lengths of $10^{15}$ cm where the velocity is 20 km sec$^{-1}$ and the velocity change along this length is less than 0.5 km sec$^{-1}$. It may be possible to construct collapsing-cloud models to satisfy the constraints on the OH maser; however, these would probably be somewhat artificial. Therefore, confronted with the problem of obtaining long path lengths and considering the evidence for evolved stars presented in the following paragraphs, we will take no further consideration of the collapsing model.

One model that seems to provide the proper conditions for the OH maser and also fits the observed characteristics of the emission is that of a star with an expanding atmosphere. One specific case of this model could be a very luminous red-giant star in the later stages of its evolution when it is expanding to a very large diameter and matter is streaming from the star into space as in the solar wind. The material of the outer layers of the star is being forced away by the radiation pressure of the star at a velocity greater than its escape velocity: $v_e = \sqrt{(2GMr^{-1})}$ km sec$^{-1}$. For a star of 2 $\mathfrak{M}_\odot$ at a radius of $2 \times 10^{15}$ cm, a lower limit to the streaming velocity is 6 km sec$^{-1}$. This is close to the observed radial velocities of 10–40 km sec$^{-1}$ (Table 9). Rose (1969) has calculated a stellar atmosphere for an expanding red giant with a luminosity of $10^4$–$10^5$ $L_\odot$, and finds that at a radius of $10^{15}$ cm the density is $10^{-16}$ g cm$^{-3}$, the temperature is 600° K, and the radial velocity is 20 km sec$^{-1}$ and is essentially constant over a length of $10^{15}$ cm.

The OH clouds could be located in a spherical region at $10^{15}$ cm from the central star. with a thickness of $10^{15}$ cm, where the conditions of density, IR flux, velocity, and temperature are satisfied for the IR-pumped OH maser. In this region, the stellar material flows through, driven by radiation pressure, and with a small amount of turbulence it could form separate clouds of material from which the OH masering originates. These individual features might be seen from both the front and back of the expanding shell. A map of the emission features could show them to be randomly distributed over a circle, if the emission angles are large. Most likely, the OH clouds would not be spherically distributed, and the OH features might be concentrated in one region. In fact, if there were a small rotation, the source might be an expanding disk, and the OH features could then be randomly distributed around a ring.

One observational fact that does not fit this simple expanding model is that in three cases the velocity of the star, as measured from optical absorption features, is very near the high-velocity group of OH emission features. The three stars are NML Tau, VY CMa, and R Aql (Hyland, Becklin, Frogel, and Neugebauer 1970; Hyland, Becklin, Neugebauer, and Wallerstein 1969; Merrill 1942). In the case of VY CMa there are "shell" absorption lines corresponding to the lower OH velocity. Thus, the simple expanding model must be modified. A general model which would explain the observed properties would be one in which some of the OH clouds near the star were moving at the velocity of the star and another concentration of OH clouds further from the star was moving away in an ejected shell. The received OH emission would originate from the side of the star toward the Earth, and the masering clouds could be amplifying the 18-cm radiation from the star. Another variation of this configuration would be to have a shock wave in the atmosphere of the star which could allow the lower-velocity OH clouds to be close to the star and the clouds moving at the velocity of the star to be further out. Clearly there are many other configurations which can be invented to explain the observed emission properties. However, all these configurations must satisfy the conditions of temperature, density, and low turbulence which are required for the near-IR–pumped OH maser. Further observational data, both optical and radio, will be required to determine the details of an expanding model.

One observational test of the expanding model versus the rotating model would be to observe the changes in radial velocity of the features as a function of time. This expanding model with the material streaming through the masering region could be distinguished by only a very small change in mean velocity over a long period of time. This time scale could be of the order of $10^4$ years, the evolutionary time of the star. However, depending on the connection of the OH clouds and the atmosphere of the star it might be possible to observe small periodic changes in the radial velocity during the cycle of the variable star as is observed in the optical lines. This possibility will be checked in future observations. As previously noted for the rotational model, changes in velocity might be observed in a few years. Individual features in the expanding model could change, however, because the streaming of the material could change the structure of the clouds. The time scale for these changes would be $T \sim l_0/V_r = 10^{15}/2 \times 10^6 \sim 20$ years. Also, the entire group of emission features could change in time because of the strength of the IR pump, as discussed in § IV*b*.

There are several other facts favoring the identification of these very red IR sources as evolved red giants or supergiants. First, in optical and IR observations it has been noted that the spectral features of many of these stars are similar to those of M6–M8 types (Wing *et al.* 1967; Johnson 1968; Hyland, Becklin, Frogel, and Neugebauer 1970). Second, many of these sources are variables similar to those of other giant stars. Third, the luminosities of these stars are great. The only sources with complete published spectral data are NML Cyg and VY CMa. If the distance to NML Cyg is 500 pc, then this source has a luminosity of $5 \times 10^4\ L_\odot$ (Stein *et al.* 1969). At this distance the diameter of the IR source would be of the order of $10^{15}$ cm, which is $10^4\ D_\odot$—truly a giant (Stein

*et al.* 1969). Hyland, Becklin, Neugebauer, and Wallerstein (1969) have estimated the total luminosity of VY CMa to be $4 \times 10^4\ L_\odot$. A final fact favoring the evolved red-giant theory for most of these sources is that they are not concentrated in the plane and have an average galactic latitude of 19°, as would be the case with Population II objects. From the OH model, it is also possible to calculate a mass loss equal to $4\pi r^2 \rho V_r$, or $\sim 10^{-6}\ \mathfrak{M}_\odot$ year$^{-1}$. This is a rate somewhat greater than that of normal red giants but somewhat less than that of planetary nebulae.

## V. CONCLUSIONS

The results of observations of OH associated with IR stars have been presented. Twelve percent of the IR stars observed have OH emission associated with them. The OH emission is strongest at the 1612-MHz satellite-line frequency, and this emission occurs in two main velocity ranges. No emission was detected at the 1720-MHz satellite-line frequency. Considering the properties of this emission, we concluded that the OH emission probably arises from a cloud of OH molecules which has been pumped by near-IR radiation to become a partially saturated maser.

The objects that can best explain the observed IR and OH properties of these sources are expanding, luminous, evolved, red-giant stars. The atmosphere of the star could be expanding as a stellar wind because of the radiation pressure from the central star, and the OH masering clouds are located in the outer parts of the atmosphere at a radius of $10^{15}$ cm where the conditions for the OH maser—low densities ($10^{-17}$ g cm$^{-3}$) and low temperatures (600° K)—are found. It was assumed that the central source appeared as a 1000° K blackbody to the OH cloud and subtended a solid angle of approximately 1 sterad.

The key to which IR stars have OH emission has not been found, although the conditions of redness and variability seem to be necessary but not sufficient. A probable explanation as to why only 12 percent of these red stars had detectable OH emission is that the limit of detection in the observations was 1–2 flux units and many sources may have been weaker. The negative OH observations of the young T Tauri stars indicate, however, that these stars do not provide the necessary conditions for the OH/IR masering.

This is the first class of OH sources which has been identified with stellar objects—red-giant or supergiant stars. This not only provides information on the OH masering process but will also provide information on the red-giant stars themselves (for example, measurements of conditions in their outer atmospheres) and on their mass loss. From one possible model presented here, the mass loss from these objects was calculated to be $10^{-6}$ $\mathfrak{M}_\odot$ year$^{-1}$. Interestingly enough, this rate of mass loss is intermediate between the value of ordinary red-giant stars and planetary nebulae.

We would like to thank Drs. E. E. Becklin, A. R. Hyland, and G. Neugebauer of the California Institute of Technology for their cooperation in supplying us with the positions of the IR stars and for reviewing this manuscript. We also acknowledge helpful discussions with Dr. M. M. Litvak. H. F. Hinteregger, and C. A. Zapata assisted with VLBI measurements. We thank the staffs of the National Radio Astronomy Observatory and the Haystack Microwave Research Facility, Lincoln Laboratory, MIT, for facilities and technical support. We thank Dr. J. A. Ball and the staff of the Agassiz station, Harvard College Observatory, for making the special observations of IRC—20197. The NRAO is operated by Associated Universities, Incorporated, under contract with the National Science Foundation.

## REFERENCES

Allen, C. W. 1963, *Astrophysical Quantities* (2nd ed.; London: Athlone Press).
Ball, J. A., and Meeks, M. L. 1968, *Ap. J.*, **153**, 577.
Bare, C., Clark, B. G., Kellermann, K. I., Cohen, M. H., and Jauncey, D. L. 1967, *Science*, **157**, 189.

Becklin, E. E., and Neugebauer, G. 1967, *Ap. J.*, **147**, 799.
Eliasson, B., and Bartlett, J. F. 1969, *Ap. J.* (*Letters*), **155**, L79.
Ellder, J., Ronnang, B., and Winnberg, A. 1969, *Nature*, **222**, 67.
Forbes, F. F. 1967, *Ap. J.*, **147**, 1226.
Hazard, C., Mackey, M. B., and Shimmins, A. J. 1963, *Nature*, **197**, 1037.
Heer, C. V., and Settles, R. A. 1967, *J. Mol. Spectrosc.*, **23**, 448.
Herbig, G. H. 1962, *Adv. Astr. and Ap.*, Vol. **6**.
———. 1966, in *Vistas in Astronomy*, Vol. **8**, ed. A. Beer and K. Aa. Strand (New York: Pergamon Press).
———. 1968, *Ap. J.*, **152**, 439.
Hilgeman, T. 1969, private communication.
Hyland, A. R., Becklin, E. E., Frogel, J. A., and Neugebauer, G. 1970, *Ap. J.* (in preparation).
Hyland, A. R., Becklin, E. E., Neugebauer, G., and Wallerstein, G. 1969, *Ap. J.*, **158**, 619.
Johnson, H. L. 1968, *Ap. J.* (*Letters*), **154**, L125.
Johnson, H. L., Mitchell, R. I., Iriarte, B., and Wisniewski, W. Z. 1966, *Comm. Lunar and Planet. Lab.*, N63, **4**, 99.
Kellermann, K. I., and Pauliny-Toth, I. I. K. 1969, *Ap. J.*, **157**, 1.
Larson, R. B. 1968, unpublished Ph.D. thesis, California Institute of Technology.
Litvak, M. M. 1969*a*, *Ap. J.*, **156**, 471.
———. 1969*b*, private communication.
Low, F. J. 1969, paper presented at the conference on IR and Microwave Radiation from Nebulae and Extragalactic Systems held at the Institute of Theoretical Astronomy, Cambridge University.
Mendoza, E. E. V. 1968, *Ap. J.*, **151**, 977.
Merrill, P. W. 1942, *Ap. J.*, **94**, 171.
Moran, J. M., Burke, B. F., Barrett, A. H., Rogers, A. E. E., Ball, J. A., Carter, J. C., and Cudaback, D. D. 1968, *Ap. J.* (*Letters*), **152**, L97.
Neugebauer, G. 1969, private communication.
Neugebauer, G., and Leighton, R. B., 1969, *Two-Micron Sky Survey: A Preliminary Catalog* (Washington: National Aeronautics and Space Administration).
Neugebauer, G., Martz, D. E., and Leighton, R. B. 1965, *Ap. J.*, **142**, 399.
Plaut, L. 1965, in *Galactic Structure*, ed. A. Blaauw and M. Schmidt (Chicago: University of Chicago Press).
Raimond, E., and Eliasson, B. 1967, *Ap. J.* (*Letters*), **150**, L171.
Rogers, A. E. E., and Barrett, A. H. 1968, *Ap. J.*, **151**, 163.
Rose, W. 1969, private communication.
Shklovskii, I. S. 1967, *Astr. Circ. U.S.S.R.*, **424**, 1.
Stein, W. A., Gaustad, J. E., Gillett, F. C., and Knacke, R. F. 1969, *Ap. J.* (*Letters*), **155**, L177.
Turner, B. E. 1967, unpublished Ph.D. thesis, Department of Astronomy, University of Calif., Berkeley.
———. 1969, *Ap. J.*, **157**, 103.
Turner, B. E., Buhl, D., Churchwell, E. B., Mezger, P. G., and Snyder, L. E. 1970, *Astr. and Ap.* (in press).
Ulrich, B. T., Neugebauer, G., McCammon, D., Leighton, R. B., Hughes, E. E., and Becklin, E. 1966, *Ap. J.*, **146**, 288.
Wilson, W. J., and Barrett, A. H. 1968, *Science*, **161**, 778, 23.
Wing, R. F., Spinrad, H., and Kuhi, L. V. 1967, *Ap. J.*, **147**, 117.
Wisniewski, W. Z., Wing, R. F., Spinrad, H., and Johnson, H. L. 1967, *Ap. J.* (*Letters*), **148**, L29.